A Fast Cloud Overlap Parameterization for Microwave Radiance Assimilation

CHRISTOPHER W. O'DELL*

Department of Atmospheric and Oceanic Sciences, University of Wisconsin—Madison, Madison, Wisconsin

PETER BAUER

European Centre for Medium-Range Weather Forecasts, Reading, United Kingdom

RALF BENNARTZ

Department of Atmospheric and Oceanic Sciences, University of Wisconsin—Madison, Madison, Wisconsin

(Manuscript received 26 April 2006, in final form 19 September 2006)

ABSTRACT

The assimilation of cloud- and rain-affected radiances in numerical weather prediction systems requires fast and accurate radiative transfer models. One of the largest sources of modeling errors originates from the assumptions regarding the vertical and horizontal subgrid-scale variability of model clouds and precipitation. In this work, cloud overlap assumptions are examined in the context of microwave radiative transfer and used to develop an accurate reference model. A fast cloud overlap algorithm is presented that allows for the accurate simulation of microwave radiances with a small number of radiative transfer calculations. In particular, the errors for a typical two-column approach currently used operationally are found to be relatively large for many cases of cloudy fields containing precipitation, even those with an overall cloud fraction of unity; these errors are largely eliminated by using the new approach presented here, at the cost of a slight increase in computation time. Radiative transfer cloud overlap errors are also evident in simulations when compared to actual satellite observations, in that the biases are somewhat reduced when applying a more accurate treatment of cloud overlap.

1. Introduction

There is currently a need for fast yet accurate radiative transfer (RT) models for scattering atmospheres. Numerical weather prediction (NWP) models rely increasingly on assimilation of radiance data directly, rather than derived products (English et al. 2000). Operational centers are beginning to assimilate microwave and infrared radiances under all weather conditions, instead of under clear skies only, as is currently done (Greenwald et al. 2002). For example, recently the European Centre for Medium-Range Weather Forecasts (ECMWF) has begun assimilation of microwave radiances under precipitating conditions using an Eddington model (Bauer et al. 2004, 2006a,b), and other efforts are under way elsewhere (Deblonde et al. 2007). Future assimilation efforts may also include the assimilation of infrared radiances under cloudy conditions (Heilliette and Garand 2007).

To produce a successful assimilation, it is necessary to be able to accurately simulate radiances based upon model data. However, because NWP models have only a finite horizontal resolution, any subgrid-scale cloud process must be parameterized within the radiative transfer model. Therefore, cloud liquid water and ice contents as well as liquid and frozen precipitation fluxes represent grid box averages. No explicit information on the spatial distribution of these quantities inside the grid box is available other than the profile of cloud fraction. The NWP model cloud fraction is usually parameterized as a function of layer humidity as is cloud liquid water.

The most important effect on microwave radiative transfer can be expected to originate from the combination of cloud coverage and precipitation fluxes between layers (Jakob and Klein 2000). To treat the prob-

* Current affiliation: Department of Atmospheric Science, Colorado State University, Fort Collins, Colorado.

Corresponding author address: Christopher W. O'Dell, Department of Atmospheric Science, Colorado State University, 200 W. Lake St., Fort Collins, CO 80523.
E-mail: odell@atmos.colostate.edu

DOI: 10.1175/2006JAS2133.1

lem of cloud overlap, the general approach is to represent an NWP model-generated profile as multiple independent profiles, or columns, each containing binary clouds; that is, each model layer is considered either fully clear or fully cloudy within a column. Next, top-of-atmosphere (TOA) radiances or brightness temperatures are evaluated using a plane-parallel, multiple-scattering radiative transfer calculation for each column. These TOA radiances are then averaged to simulate what is observed by a satellite instrument for that profile. Because of the nonlinear nature of radiative calculations, many columns and corresponding radiative transfer simulations are in principle necessary to simulate a single radiance from a partially cloudy pixel. Such an approach is prohibitively expensive for most assimilation systems, which can typically afford at most two or three radiative transfer calculations per profile.

A faster, more approximate scheme was provided in Bauer et al. (2006c, hereafter B06) and is part of the widely used Radiative Transfer for the Television and Infrared Observation Satellite (TIROS) Operational Vertical Sounder (TOVS) (RTTOV) radiative transfer package (Saunders et al. 2005). The full microwave scattering package is called RTTOV-SCATT and is fully described in B06. In the RTTOV-SCATT approach to treating cloud overlap, a profile is divided into two columns, one clear and one cloudy, with the weight of the cloudy column proportional to the maximum cloud fraction in the profile. Thus, only one clear-sky (nonscattering) and one cloudy-sky (scattering) plane-parallel RT calculation is necessary. This approach to treating the cloud fraction information is quite numerically efficient but will be shown below to often have limited accuracy. To our knowledge no other models currently treat the issue of cloud overlap specifically within microwave radiative transfer models.

The present work will characterize the accuracy of the RTTOV-SCATT approach and other simple methods of treating cloud overlap as applied to the problem of microwave radiative transfer, and will introduce a new cloud overlap approach that, though not quite as computationally efficient as the RTTOV-SCATT scheme, is roughly an order of magnitude more accurate. Essentially the same cloud overlap problem was addressed in Collins (2001) in deriving a fast radiative transfer approach for the calculation of shortwave and longwave fluxes and heating rates in climate models, given a particular cloud overlap assumption (such as maximum-random). In that study, however, the plane-parallel assumption was not an issue because of the large horizontal size of the climate model grid boxes. However, the size of NWP grid boxes is relatively smaller, and thus this work also attempts to characterize the 3D errors incurred by the plane-parallel assumption.

The rest of this article is organized as follows. Section 2 describes the profile database that will serve as the test bed for our studies, while section 3 formulates the reference overlap approach against which to test fast cloud overlap models, and also discusses possible errors introduced by the reference model assumptions. Next, section 4 describes several more computationally efficient approaches to serve as fast alternatives to the reference scheme. Section 5 characterizes the accuracy of the fast models as compared to the reference overlap model, whereas section 6 examines the full forward-model errors as compared with actual microwave observations. A brief discussion of the results is given in section 7.

2. Base profiles and microphysics

The profile datasets were drawn from the ECMWF efforts to assimilate cloud- and precipitation-affected radiances from several Special Sensor Microwave Imager (SSM/I) instruments aboard the U.S. Defense Meteorological Satellite Program (DMSP) satellites (Bauer et al. 2006a,b). The SSM/I has seven microwave channels at the frequencies 19.35, 22.235, 37.0, and 85.5 GHz; except for 22.235 GHz, each band has separate channels for both vertical (V) and horizontal (H) polarization (Hollinger et al. 1987). With the exception of section 6, this study utilizes atmospheric profiles generated from the ECMWF global NWP model 6-h forecasts at roughly 40-km horizontal resolution, chosen for their representativeness of different precipitation regimes. Two separate sets of profiles were used: 24 000 profiles were taken from the Atlantic Ocean in July 2004, hereafter referred to as the summer profiles, and 10 000 profiles were taken from the Atlantic Ocean in January 2004, referred to as the winter profiles; see Di Michele and Bauer (2006) for details. All profiles are composed of 60 vertical atmospheric layers. Figure 1a shows the distribution of $C_{\max}$, the maximum layer cloud cover fraction of a profile. Both the winter and summer profile sets are similar, with most of the selected profiles having at least one fully cloud-covered layer. Figures 1b,c display the distribution of the rain and snow water path, which are simply the column-integrated mass of rain and snow, respectively. The summer profiles tend to have more rain than the winter cases, while the distributions for snow in each are quite similar. This is probably due to the larger number of strongly convective cases in the summer profiles generating frozen precipitation at relatively high altitudes, roughly matching the lower-altitude frozen precipitation in the winter profiles.

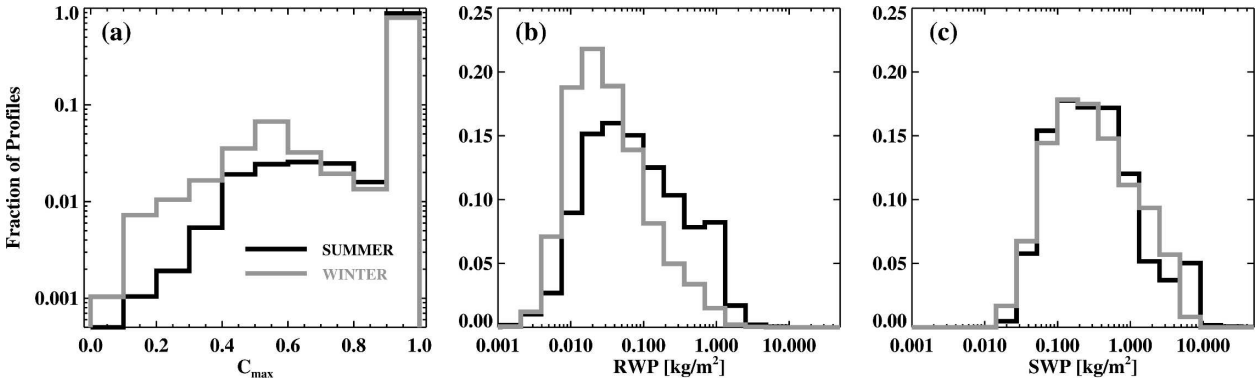

FIG. 1. Distributions of some variables for the sets of profiles used in this study. (a) The distribution of the maximum cloud cover fraction (C_{max}), (b) the distribution of the rainwater path (RWP), and (c) the distribution of snow water path (SWP). Black lines are for the summer profiles, while gray lines are for the winter profiles.

To conduct radiative transfer simulations, optical properties of the relevant atmospheric variables were calculated at the SSM/I frequencies. The profiles of pressure, temperature, water vapor, cloud liquid water, and cloud ice were used to obtain absorption coefficients for each layer using the algorithms of Rosenkranz (1998) and Liebe et al. (1991). For cloud water and ice, spherical monodisperse drop sizes of 10 and 20 μm are assumed, respectively, and their optical properties were calculated using the Rayleigh approximation (this is valid even up to frequencies of 183 GHz for the sizes assumed). Profiles of rain and snowfall rates were converted to optical properties of extinction, single-scatter albedo, and asymmetry parameter using the precipitation microphysics model of Bennartz and Petty (2001) with a size ratio of 1. This model assumes spherical particles, a Marshall–Palmer drop size distribution for rain, and a modified gamma distribution for snow. Mie theory was then used to calculate the optical properties. The lower surface was taken to be ocean, with emissivity calculated using the fast ocean surface emissivity model (FASTEM) version 2 (Deblonde and English 2001). For plane-parallel calculations, the radiative transfer model employed[1] was the Successive Order of Interaction (SOI) model (Heidinger et al. 2006; O'Dell et al. 2006). The SOI model is generally accurate to a few tenths of a kelvin, which is more than sufficient for the purposes here.

3. Reference model

To assess the accuracy of fast, approximate cloud overlap parameterizations, it is first necessary to describe an "ideal" or *truth* forward radiative transfer model. In this section, different sets of assumptions will be addressed in the process of formulating a suitable reference model for the treatment of cloud overlap, against which to test more approximate, faster schemes.

a. The independent column approximation

The basic task in order to treat cloud overlap within the radiative transfer context is to accurately characterize the subgrid-scale variability of a given model pixel (or profile), as encapsulated within the cloud fraction variable, that actually affects the radiative transfer. We begin by working within the framework of the independent column (IC) approximation,[2] which divides a pixel into N_c columns and performs a separate, plane-parallel radiative transfer calculation on each column independent of the other columns. This approach is commonly adopted in the literature as a good reference model, for example in Collins (2001) where a fast parameterization of cloud overlap is introduced in order to calculate shortwave and longwave radiative fluxes in climate models. Later in this section, an attempt will be made to quantify the errors associated with the IC assumption.

Within the IC framework, there are three primary sets of assumptions that must be addressed:

1) Column width assumptions: Are the columns all equally wide, or are some columns wider than others? The column widths are proportional to the weights assigned to each column in the final radiance average.
2) Cloud overlap assumptions: How are cloud particles to be distributed within a layer?

[1] Except in section 6, where an Eddington model is employed.

[2] The IC approximation is often referred to as the independent pixel approximation (IPA) in the literature.

3) Precipitation distribution assumptions: How is the precipitation within a layer to be distributed among the different columns?

Regarding column width, we make the simplifying assumption that all of the ICs are equally wide. For a profile with N_c ICs, each column then occupies a width of $1/N_c$ of a grid box. This also implies that the resultant radiances calculated for each column are equally weighted in the calculation of the overall radiance for the profile.

Regarding cloud overlap, there are three typical simplistic approaches used: maximum (MAX), random (RAN), and maximum-random (MR) overlap. MAX overlap implies a minimum in the overall cloud fraction for the pixel, while RAN assumes completely random overlap for all cloudy layers. MR overlap uses maximum overlap for a vertically contiguous cloud object, but random overlap for cloudy layers separated by noncloudy layers. A good deal of work has been performed in assessing which overlap scheme most accurately represents reality, based both on observations (e.g., Tian and Curry 1989; Hogan and Illingworth 2000; Mace and Benson-Troth 2002; Stephens et al. 2004; Willen et al. 2005) and on cloud-resolving models (Oreopoulos and Khairoutdinov 2003; Wu and Liang 2005), as well as what the effects of cloud overlap assumption are on general circulation models (e.g., Morcrette and Jakob 2000; Collins 2001). There is some evidence that the maximum-random approach is supported by observations (Tian and Curry 1989; Stephens et al. 2004; Willen et al. 2005). Other studies have found that the random overlap assumption for layers separated by noncloudy layers is supported by the observations (Mace and Benson-Troth 2002), but that the overlap correlation between vertically continuous layers decays exponentially with a vertical decorrelation length of roughly 1.5–3 km (Hogan and Illingworth 2000; Oreopoulos and Khairoutdinov 2003). Both for simplicity and to match the scheme used by the ECMWF NWP model, the MR scheme shall be adopted for the reference RT model in this work. It is therefore important to note that the particular cloud overlap assumption (such as maximum-random) is not being tested in this work; only the treatment of cloud overlap within the radiative transfer is under investigation, and is thus analogous to the work by Collins (2001) in deriving a fast radiative transfer approach for calculation of shortwave and longwave fluxes and heating rates in climate models, given the same cloud overlap problem.

Finally, the issue of the distribution of precipitation must be addressed. A simple first approach for this has been given in the IC reference model described in B06 that was used to test the accuracy of the faster RTTOV-SCATT scheme. In this approach, the density of all precipitates (cloud water, cloud ice, rain, and frozen precipitation) in a given layer simply follows that of the cloud location. For each layer, the total mass of each species is conserved. This model has the benefit of simplicity but is unphysical; it does not allow precipitation to "fall out" of clouds. The cloud and precipitation distribution scheme adopted for the present work is based on the above scheme but is more physically based. The cloud fraction, as well as the cloud water and ice, are distributed using maximum-random overlap. However, precipitation is distributed according to the following rules:

- Precipitation is distributed one layer at a time, starting with the topmost layer and descending through the atmosphere.
- If a layer has *less* precipitation than the previous layer, the precipitation is distributed in proportion to that of the previous layer.
- If a layer has *more* precipitation than the previous layer, an amount of precipitation equal to that contained in the previous layer is distributed as in the previous layer; the remainder is distributed uniformly among the cloud-filled areas within the layer.

As in the B06 approach, the mass of each species is preserved for each layer. This new approach is more consistent with the actual moist physics, however, as it allows precipitation to fall out of cloud layers and maintain its horizontal distribution (horizontal winds are neglected). Both approaches are illustrated in Fig. 2.

b. Reference model errors

If one adopts the philosophy that the reference model should be truly error free, then it may seem initially desirable to make no particular assumptions regarding its formulation. A very general and accurate reference model would in principle have an infinite number of nonindependent (or interacting) columns, with the clouds and precipitation distributed in three dimensions according to the rules described above. Then a fully three-dimensional (3D) radiative transfer calculation, such as from a Monte Carlo model, could be performed in order to determine the upwelling radiances for each pixel, taking into account both the observation direction zenith and azimuth. However, in reality the reference model must have a finite number of columns, and in order to not be overly computationally expensive, the plane-parallel approximation is typically used, rather than a fully 3D calculation. Both of these assumptions are now examined in more detail.

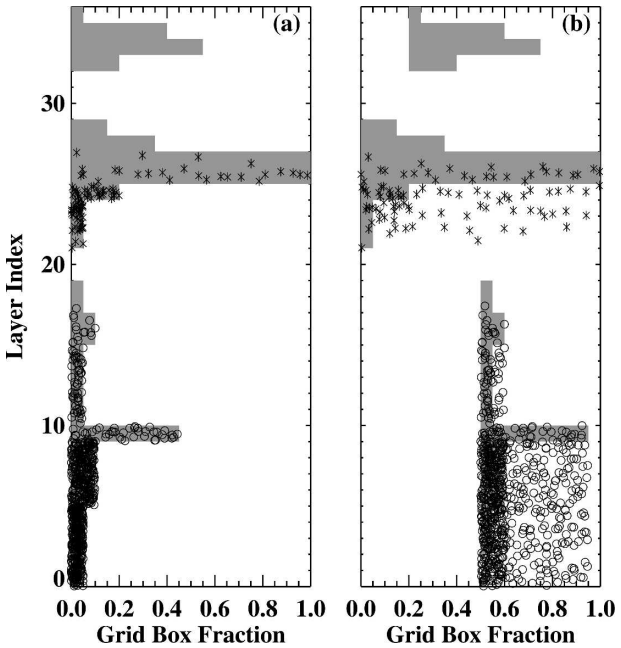

FIG. 2. Comparison of two different schemes for distributing clouds and precipitation in the reference model. Each scheme assumes 20 independent columns. Cloud presence is indicated by gray shading, whereas rain is denoted by open circles and snow by stars: (a) scheme from B06, (b) scheme for this paper.

Let us first address the question of how many equally weighted columns are necessary within the context of the IC approximation to achieve suitable accuracy. Figure 3 shows the bias and bias-corrected RMS error in the upwelling, TOA brightness temperature (TB) for the radiative transfer assuming MR overlap as a function of N_{IC}, the number of independent columns used. Only H polarization is displayed, as H-polarization errors are nearly always worse than V-polarization errors. This is because of the fact that V-polarization has a higher ocean surface emissivity in the microwave, and hence a smaller dependence on atmospheric properties. The reference was taken to have $N_{IC} = 200$. The figure shows that the RMS error associated with having a finite number of ICs falls roughly like $1/N_{IC}$. By $N_{IC} = 100$, the RMS is below 0.15 *K* and the bias has fallen well below 0.01 K. Though only 19- and 85-GHz calculations are shown in Fig. 3a, these conclusions hold for all SSM/I channels. Going beyond simple bias and RMS error, Fig. 3 shows the error histogram for all SSM/I channels taken simultaneously, for both V and H polarization. This confirms the general smallness of the errors at $N_{IC} = 100$; all of the V-polarization radiances and 99.94% of the H polarization were below 1 K.

Because the levels of error for cloud overlap will in general be much higher than this, $N_{IC} = 100$ with maximum-random overlap is taken to be a suitable reference model. As a side study, tests (not shown) comparing a 100-IC model using MR versus MAX cloud overlap schemes were performed in order to evaluate the microwave radiance differences produced between these two cloud overlap schemes. While some profiles had differences of several kelvin, the overall RMS difference ranged from 0.011 K at 19 GHz to 0.20 K at 85 GHz, indicating that in general, the differences in the microwave between these two cloud overlap schemes as applied to the radiative transfer are not large. Never-

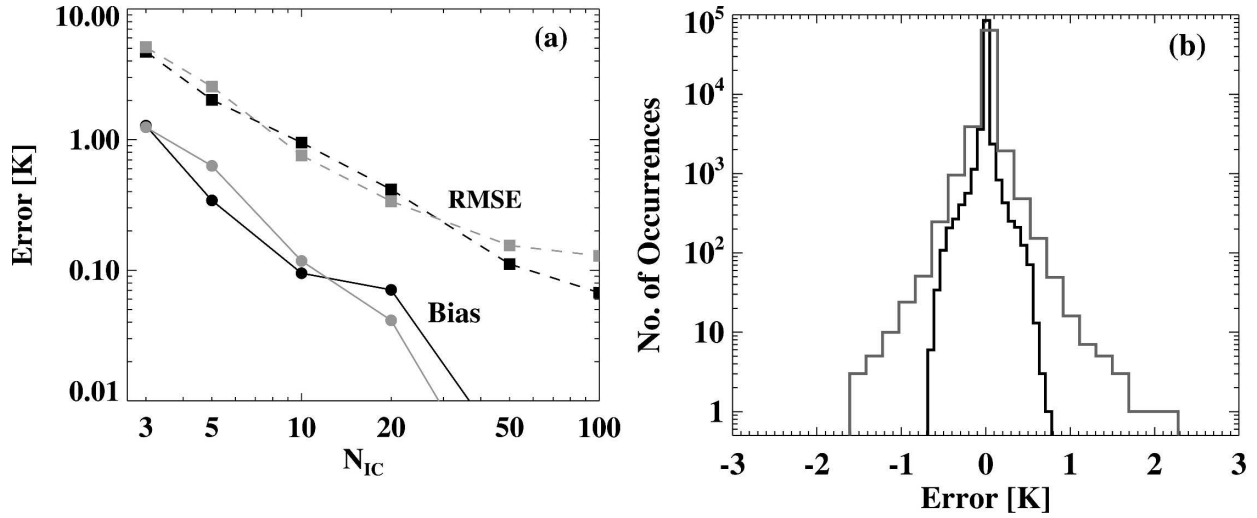

FIG. 3. Errors due to a finite value of N_{IC}, the number of independent columns. (a) Error statistics at 19 GHz (black) and 85 GHz (gray) vs N_{IC} for H-polarization. Both the bias (solid lines) and bias-corrected RMS (dashed lines) of the errors are displayed. (b) Histogram of errors for $N_{IC} = 100$ at all SSM/I frequencies, for both V (black) and H (gray) polarizations.

theless, the MR overlap scheme was kept within the reference model for consistency with the NWP model that generated the profiles.

c. Errors due to the IC assumption

The errors discussed above assume that the underlying IC approach is correct given a large number of columns. Let us now briefly attempt to quantify the error associated with the independent column, plane-parallel assumption itself. As a more realistic model, a 3D approach was taken. This model is by no means unique; it is only meant to provide an idea of the rough level of error introduced by the IC assumption. In this 3D approach, profiles were partitioned horizontally onto a two-dimensional grid of interacting columns, based on the cloud fraction in each vertical layer (as in the IC case). As a baseline, a 9×9 grid of columns was used. MR vertical cloud overlap was employed with the caveat that the lowest cloud object was centered with respect to the overall profile; all other cloud objects were placed randomly. Two sets of calculations were performed assuming horizontal pixel sizes of 20×20 and 40×40 km.

When partitioning cloudy cells within a vertical layer, an extra complexity arises for two horizontal dimensions; the assumption of continuity of the cloud object within the layer is no longer enough to uniquely determine which columns are cloudy within the layer. We make the simplifying assumption that the cloud object has a minimum areal extent within the layer; this tends to make square or circular-shaped clouds, as opposed to more one-dimensional cloud objects. Figure 4 shows the cloud distribution of the sample profile of Fig. 2 for the 3D approach using MR cloud overlap. In this particular case, three separate cloud objects are present. The distribution scheme for precipitation is the same physical approach as in the IC scheme. Another issue is that the boundary conditions are not uniquely defined, as the profile is considered in isolation from its neighbors. We make the simplifying assumption that the boundary conditions are continuous; cells outside the domain take the properties of the nearest cell within the domain.

To conduct the radiative transfer, a Monte Carlo or other fully three-dimensional model would be most appropriate, but would also be extremely computationally demanding. We employ the SOI model as before, but in a slant-path mode. Calculations comparing this model to a reverse Monte Carlo model (Petty 1994) show that it typically removes $\gtrsim$90% of the errors incurred by a plane-parallel model (O'Dell et al. 2006). Use of this model, while not ideal, nonetheless allows a rough characterization of the 3D errors incurred by the IC assumption. Finally, note that the upwelling TB at the top-of-atmosphere will depend on the observation azimuth angle for all nonnadir observations. Because the azimuthal dependence is somewhere arbitrary (being dependent on the random element of the MR approach), TBs were calculated for eight equally spaced azimuth angles and averaged.

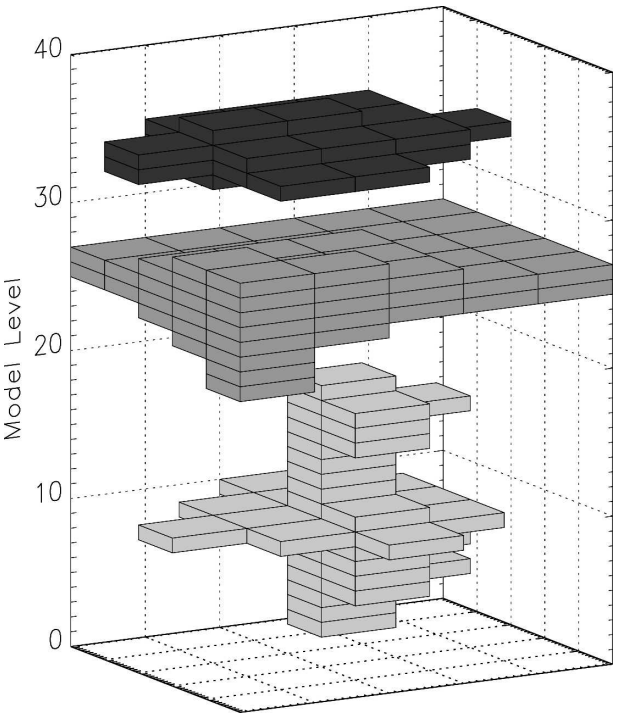

FIG. 4. Illustration of 3D cloud overlap for profile from Fig. 2. Maximum-random overlap was applied in the vertical; cloud objects are contiguous in the horizontal, and attempt to occupy a minimum horizontal area for each layer.

The results of this calculation on the summer ocean profiles are shown in Table 1, which compares 3D calculations at 20- and 40-km horizontal pixel size to results from the IC approximation with $N_{IC} = 100$. At 20-km resolution, the errors may seem surprisingly

TABLE 1. Approximate 3D errors (K) due to the IC assumption.

	20 km			40 km		
Channel	Bias	RMS	Max error*	Bias	RMS	Max error*
19 V	−0.8	2.8	−20.1	−0.3	1.0	−8.6
19 H	−1.3	4.8	−33.1	−0.7	2.2	−17.5
22 V	−0.5	1.6	−11.6	−0.1	0.4	−3.5
37 V	−1.1	3.5	−24.6	−0.4	1.0	−9.7
37 H	−1.9	6.0	−38.1	−1.0	2.7	−20.7
85 V	−1.3	3.0	−24.6	−0.1	0.5	−5.3
85 H	−1.8	3.7	−28.3	−0.4	0.8	−7.7

* Largest error, independent of sign.

large. The IC assumption generally has a negative bias for all SSM/I channels. The negative bias is due largely to profiles with rain rates of several mm/hr near the surface, but with a cloud fraction of less than one. Under the IC assumption, there are some columns that are viewed as essentially clear, but when the 53.1° view angle of the SSM/I is taken into account along the actual slant-path view angle, there are no clear pixels. Because clear pixels over ocean generally have a lower TB, this leads to the negative bias of the IC scheme.

The errors in the IC assumption are clearly dependent on the model resolution. In the case of 40-km pixels, the errors are significantly reduced compared to the 20-km pixels, as shown in Table 1. The biases are mostly below 1 K and the RMS errors are 2–4 times better than in the 20-km case. It may seem counterintuitive that higher resolution results in *increased* forward-model error. This is a simple consequence of the plane-parallel geometry assumed for each column in the radiative transfer calculations. The plane-parallel assumption becomes more and more accurate at larger spatial scales; at smaller horizontal scales, neighboring columns have a much higher probability of interacting through multiple scattering, and thus the IC approach using independent plane-parallel calculations becomes less accurate.

Are these 3D errors too large to allow an IC approach as the basis for the reference model? We will see in section 5 that the basic cloud overlap errors are a factor of 3–5 times larger than this for the summer ocean profiles at 40 km, essentially justifying the plane-parallel assumption of the reference model at this resolution. This result was found to hold true for the winter profiles as well. However, at finer model resolutions, we must be increasingly aware of the possibility of three-dimensional radiative transfer errors.

4. Fast models

Several different approximate models for treating cloud overlap, including the RTTOV-SCATT approach, were tested as computationally efficient alternatives to the reference model. All of these models used the IC approximation, and none had more than three columns (meaning that a maximum of three radiative transfer calculations were required for any of the models). However, several of these approaches do not use equally weighted columns, though all treat clouds within the individual columns as binary objects—each layer is fully clear or fully cloudy within a column. Table 2 gives a listing of the fast models tested and their basic properties.

TABLE 2. Fast models tested in this research.

Model	Number of columns	Column weighting
1C	1	—
2C*	2	By $C_{\max}$
3EQ	3	Equal
2OP	2	Optimal scheme
3OP	3	Optimal scheme

* Scheme used within RTTOV-SCATT.

a. Simple fast models

The first three fast models tested were all relatively simplistic. The first of these models has simply one column, such that the precipitation and cloud contents are considered as averages. In this case, the cloud fraction information is not used at all. This model will be referred to as model 1C. The next fast model tested is the cloud overlap treatment used by RTTOV-SCATT, hereafter denoted model 2C, and is fully described in B06. As stated above, this is a two-column model in which one column is fully cloudy and the other is fully clear. The cloudy column receives a weight equal to the maximum cloud fraction of any of the vertical layers, referred to as $C_{\max}$. All clouds and precipitation reside entirely within the cloudy column. The overall brightness temperature TB is given simply by the weighted average of the cloudy and clear TBs, namely

$$\mathrm{TB}_{2C} = \mathrm{TB}_{\mathrm{cloudy}} C_{\max} + \mathrm{TB}_{\mathrm{clear}}(1 - C_{\max}). \quad (1)$$

The next model tested is an IC model with three equally weighted columns, denoted model 3EQ. In this model, all cloud fractions are rounded such that cloud fractions greater than zero and less than 0.5 are rounded to 0.33, fractions between 0.5 and 0.83 are rounded to 0.66, and fractions between 0.83 and 1.0 are rounded to 1.0. Example treatments of a sample profile for models 1C, 2C, and 3EQ are shown in Fig. 5.

b. The "optimal" approach

Overlap models with equally weighted columns tend to be nonoptimal because many of the columns have similar or identical properties that lead to redundant radiative transfer calculations. One approach to rectify this problem is to partition the clouds and precipitation of a given profile into many independent columns, as in the reference model, but then combine those columns into just a few "binned" columns. These binned columns will contain the average properties of the original columns. The goal is to attempt to bin together columns of similar radiative properties for the wavelengths of interest, such that averaging their properties *before* the

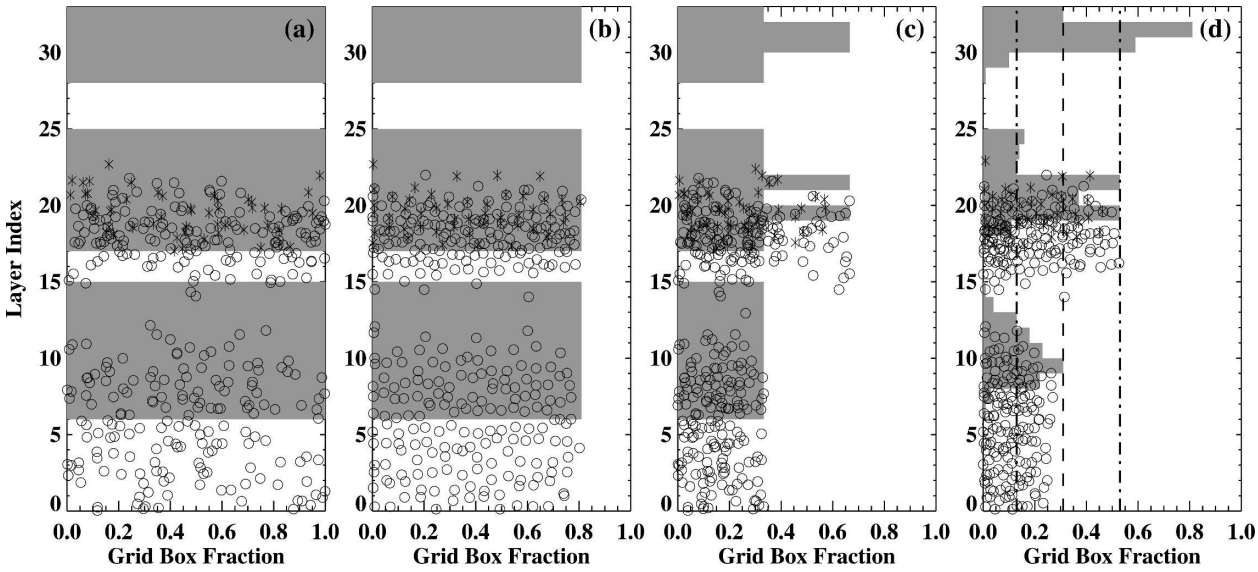

FIG. 5. Cloud and precipitation distribution schemes for the different fast models studied as applied to a sample profile. (a) The simple one-column approach (model 1C); (b) the two-column approach (model 2C), the model of RTTOV-SCATT; (c) model 3C with three equally weighted columns. (d) The optimal approach, which initially divides the profile into many columns, but combines columns with similar optical properties into two or three total bins; the dashed line shows the boundary for two bins, while the dot–dashed lines show the boundaries in the three-bin case. Note that before the radiative transfer is performed, the cloud and precipitation properties of all columns within a single bin are averaged.

radiative transfer yields similar results to averaging their upwelling TBs *after* the radiative transfer.

A simple approach was adopted to determine the radiative properties of each column upon which to base the binning strategy. It was assumed that the surface-to-space slant optical depth at some key frequency could be used as a proxy for the top-of-atmosphere TB. The steps would then be to calculate this proxy parameter for each column, and combine columns according to the similarity of their respective values of this proxy parameter. While scattering plays a role at the SSM/I frequencies, to first order the total extinction optical depth matters most in the radiative transfer, and for this reason it was chosen as an appropriate proxy variable. A frequency of 37 GHz was selected as the key frequency at which to calculate the slant optical depth. This was chosen as the "key" frequency because it has sufficient sensitivity to weak cloud water and rain contents where the overlap issue is strongest, but it suffers less from scattering and saturation than does the 85-GHz channel. Perhaps more importantly, it proved to work well for the microwave frequencies modeled in this study. The slant optical depth at 37 GHz, or τ_{37}, was approximated for each column as follows. First, the 37-GHz volume extinction coefficient k^{37}_{cloud} was estimated as

$$k^{37}_{\text{cloud}} \approx 220F_{\text{rain}} + 657(F_{\text{froz}})^{1.27} + 0.237\rho_{\text{clw}}, \quad (2)$$

where F_{rain} and F_{froz} are the liquid and frozen precipitation fluxes, respectively, in units of kg m^{-2} s^{-1}, and ρ_{clw} is the density of *liquid* cloud water in units of g m^{-3}; cloud ice was ignored as it is radiatively unimportant for the SSM/I frequencies. Note that k^{37}_{cloud} is in units of km^{-1} and is due to clouds and precipitation only. Then τ_{37} was calculated as

$$\tau_{37} \approx \sec\theta\left(G + \sum_{i=1}^{N_{\text{layers}}} k^{37}_{\text{cloud},i}\Delta z_i\right), \quad (3)$$

where θ is the observation zenith angle and Δz_i is the width of layer i in kilometers. The term G to the left of the summation is a constant offset that loosely accounts for gas absorption; a value of $G = 0.02$ was empirically determined to give good results when compared to the exact calculation of the 37-GHz optical depth. For the profiles tested in this study, Eq. (3) was found to be accurate to 30% or better over a range of about three orders of magnitude, again as compared to exact calculations of τ_{37}.

To what extent does the TB at each frequency actually depend upon the proxy variable τ_{37}? The hope is that columns with a similar value of τ_{37} will have similar TBs *at all frequencies of interest*, or at least that the resultant TBs of the columns of similar τ_{37} are somewhat linear in their optical properties, thus justifying binning them together into a single column. Figure 6

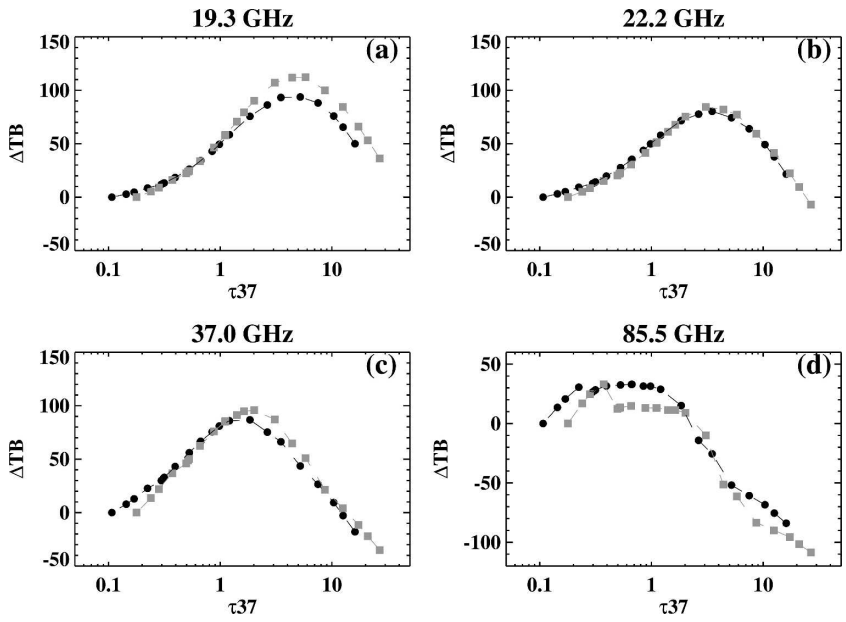

FIG. 6. Dependence of brightness temperature TB on the 37-GHz optical depth τ_{37}. Shown are the deviations ΔTB from a clear-sky TB for a sample profile containing 100 independent columns. Clouds and precipitation were distributed in the columns using the reference model scheme as described in section 3a. Black circles denote a nadir observation; gray squares denote a 53.1° observation zenith angle.

displays the results of a sample profile that has been divided into 100 independent columns using the reference model scheme. The profile was tested at observation zenith angles of both 0° (black circles) and 53.1° (gray squares), and the figure shows the resultant TBs for horizontal polarization for each of the 100 individual columns; results for vertical polarization are qualitatively similar. Many columns have the same optical properties and hence have the same top-of-atmosphere TB, explaining why there are significantly fewer brightness temperature points than columns. Note that the two curves representing different observation angles are similar for all the SSM/I frequencies.

Though Fig. 6 is only for a single profile, its results are sufficiently generic that we are somewhat justified in using τ_{37} as a proxy variable for an optimal binning strategy. Values of τ_{37} up to about 20 correspond to changes in the resultant TB, and τ_{37} can vary by a factor of several hundred among the different independent columns of a given profile. To bin together columns of similar τ_{37}, we therefore perform a simple binning on the logarithm of τ_{37}, similar to a conventional k-distribution approach in radiative transfer (e.g., Liou 2002). The optimal approach is therefore as follows:

1) Divide the profile into $N_c \gtrsim 30$ independent columns, distributing the clouds and precipitation according to the reference model scheme, with the exception that maximum cloud overlap is used.
2) For each of the N_c columns, calculate τ_{37} using Eqs. (2)–(3).
3) Divide the range of log τ_{37} into N_b equal bins, with the upper end of the log τ_{37} range restricted to have $\tau_{37} < 20$. Values of τ_{37} above this are not generally associated with changes in the output brightness temperature.
4) According to their value of log τ_{37}, associate each of the N_c columns with one of the N_b bins.
5) Average the cloud and precipitation properties of all columns of a particular bin together into a single "binned" column.
6) Perform a separate radiative transfer on each of the N_b binned columns. Weight the resultant TBs by the number of original columns in each of the binned columns.

In this study N_b was chosen as either 2 or 3, leading to models 2OP and 3OP, respectively. The choice of 30 or greater independent columns in the first step of the algorithm was chosen empirically but is somewhat arbitrary. With as few as 10 independent columns, we found the bias is negligible for all channels and the RMS is less than 1 K, as compared to the optimal approach using 100 independent columns. However, using 30–50 columns, it was found that even higher accuracy was achieved without an appreciable difference in computation time, as the overall computation speed is largely determined by the radiative transfer calcula-

TABLE 3. Fast model error statistics (K) as compared to the 100-IC reference model, except in section 6, where an Eddington model is employed. The IC approximation is often referred to as the independent pixel approximation (IPA) in the literature.

		Bias					RMS error					Maximum error				
		1C	2C	3EQ	2OP	3OP	1C	2C	3EQ	2OP	3OP	1C	2C	3EQ	2OP	3OP
Summer profiles	19 V	2.7	2.0	0.5	0.0	−0.1	8.4	6.7	2.2	0.8	0.5	43	42	16	9.1	6.9
	19 H	5.0	3.9	1.3	0.1	0.0	15.8	12.8	4.7	1.1	0.6	85	81	30	19.3	7.8
	22 V	1.1	0.8	0.0	−0.2	−0.1	3.3	2.7	1.1	1.0	0.6	22	20	11	10	7.3
	37 V	1.8	1.1	−0.5	−0.3	−0.1	5.1	4.7	2.8	1.7	0.7	34	33	24	22	10
	37 H	5.7	4.2	0.1	−0.1	0.1	15.0	12.4	3.2	1.7	0.9	82	82	27	−21	18
	85 V	−4.5	−3.5	−1.5	−0.4	−0.2	16.6	13.6	5.2	2.1	1.0	87	87	29	42	17
	85 H	−2.1	−1.7	−1.3	−0.1	−0.2	14.5	12.1	5.1	2.0	1.0	−86	−86	−29	−41	−16
Winter profiles	19 V	0.5	0.4	0.2	0.1	0.0	2.5	2.0	1.1	0.3	0.1	34	29	13	5.2	4.1
	19 H	0.9	0.7	0.4	0.1	0.0	4.4	3.5	2.1	0.6	0.2	63	53	26	11	7.2
	22 V	0.5	0.4	0.2	0.0	0.0	1.8	1.4	0.8	0.2	0.1	21	18	8.9	5.0	3.2
	37 V	1.0	0.7	0.2	0.1	0.0	3.1	2.0	1.1	0.5	0.2	31	27	16	11	8.7
	37 H	2.5	1.7	0.7	0.3	0.1	7.8	5.1	2.5	0.9	0.6	73	70	23	11	20
	85 V	−0.4	−0.5	−0.4	0.1	0.0	5.5	4.5	2.0	0.7	0.4	67	67	22	19	8.5
	85 H	3.5	2.0	0.5	0.5	0.0	7.6	5.3	2.5	1.4	0.4	−64	−64	−23	−17	−6.5

tions of the binned columns, and not by the binning calculations themselves. The optimal approach is illustrated in Fig. 5d, in which the sample profile is first divided into 100 ICs. Dividing lines separating the binned columns are shown as a dashed line in the 2OP case, and dot–dashed lines in the 3OP case.

5. Fast model performance

RT errors as compared to reference scheme

All five of the fast models were run on both the summer and winter profile sets, and compared to the 100-IC reference model. Comprehensive results for average statistics of the errors (bias, RMS error, and worst error) are listed in Table 3. The seven SSM/I channels are shown for all five of the fast models discussed previously, for both summer and winter profile sets. From these error statistics, a number of conclusions can be drawn. First, we notice that radiative transfer errors due to cloud overlap assumptions can be quite high. Indeed, the errors on the more simplistic fast models (models 1C and 2C in particular) for specific profiles can approach 90 K for the 85-GHz channels. The RMS errors (i.e., the square root of the error variance) can be well over 10 K for both models 1C and 2C. Model 3EQ is a significant improvement over the first two schemes, with errors roughly 50% smaller (it has an even larger improvement at 85 GHz). This is perhaps unsurprising, given that it uses an additional radiative transfer calculation. Model 2OP, however, is better still; its error statistics are usually a factor of two or so better than those of model 3EQ. Model 3OP performs the best of the models tested, with virtually no bias and RMS errors almost always below 1 K.

It is noteworthy that the error statistics depend upon which set of profiles is being considered; the errors are significantly worse for the summer profiles than the winter profiles. This is likely because of the fact that, even though they have similar precipitation distributions (Fig. 1b), the winter profiles have a much larger fraction of their precipitation occur in the solid phase. Solid precipitation has a smaller radiative effect for microwave frequencies less than about 100 GHz than the same mass of liquid precipitation. This tends to lead to correspondingly smaller cloud overlap radiative transfer errors.

Figure 7 shows the errors of the 2C, 3EQ, and 2OP fast models for the winter profiles, for select SSM/I channels. These errors are plotted versus $C_{\max}$ in the left-hand panels, as well as the precipitation water path (PWP) in the right-hand panels. Note that PWP is simply the sum of the rain and snow water paths. The horizontal axis of each plot has been binned, such that the plotted points represent the mean error in each bin, while the error bars correspond to ±one standard deviation. The superiority of model 2OP over the other two models remains true for virtually all values of $C_{\max}$ and PWP. Model 3OP has even smaller errors, but was left out as its errors would be barely visible in the plots. The right-hand panels demonstrate that the profiles with the highest cloud overlap errors, regardless of fast model, tend to be those profiles with a total mass of precipitation between 1 and 10 kg m^{-2}. However, for both 37 GHz (not shown) and 85 GHz, the bias can be a few kelvin for values of PWP as low as 0.05–0.10 kg m^{-2}.

The plots versus $C_{\max}$ are not particularly informative at 19 GHz; clearly the errors do not have much

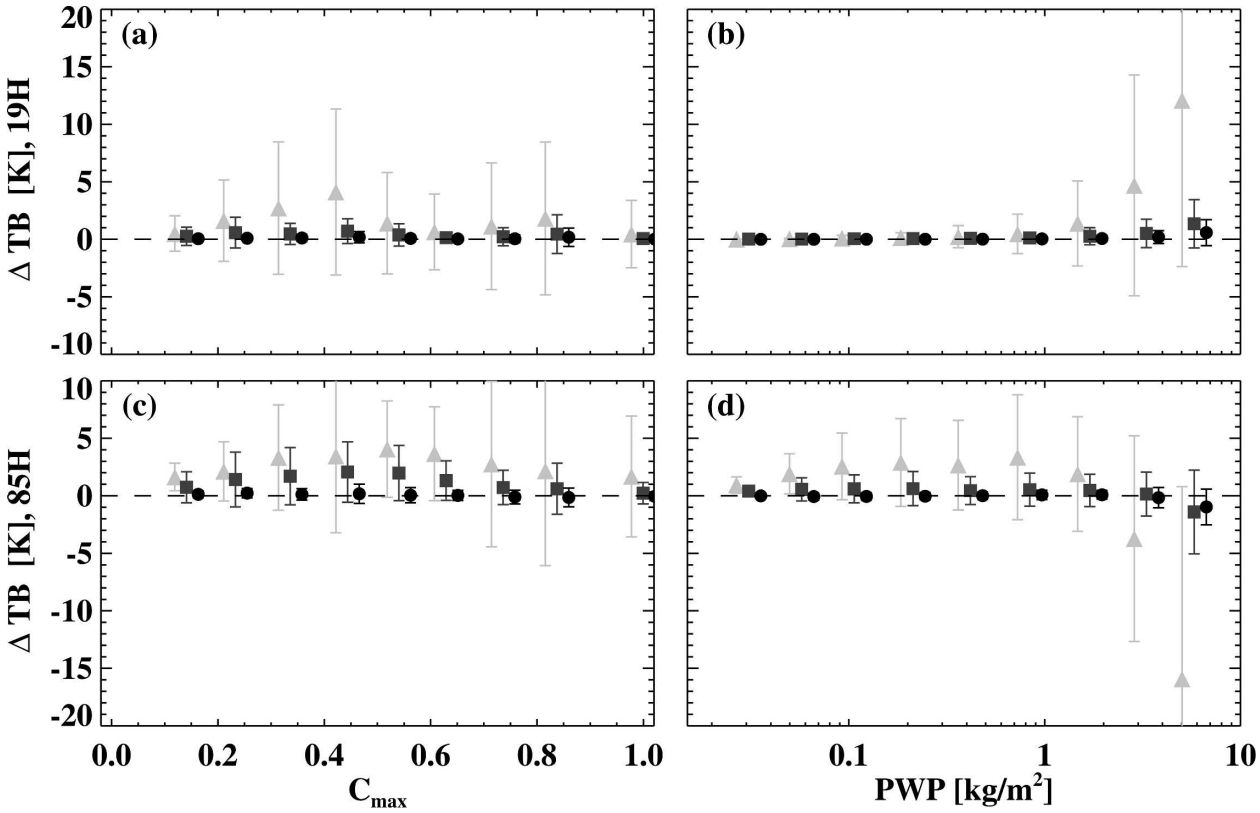

FIG. 7. Brightness temperature differences for selected fast models as compared to the reference model for the winter profiles. All plots are for horizontal polarization only; vertical polarization errors tend to be smaller: (a), (b) 19-GHz errors; (c), (d) 85-GHz errors. Panels (a) and (c) show the errors vs C_{max}, whereas (b) and (d) show the errors vs the PWP. Model 2C is shown in light gray triangles; model 3EQ is shown in dark gray squares; model 2OP is shown in black circles. The error bars represent ±1 std dev. Model 3OP was omitted as its errors would be barely visible on these plots, as compared with the models shown.

dependence upon this variable. The situation is a little different for 85 GHz, where for model 2C there is a roughly triangular dependence of the bias on C_{max}, with the worse bias occurring near $C_{max} = 0.5$. Note that this is in contrast to the findings of B06, which found a triangular-shaped bias in C_{max} for all channels. This discrepancy is likely due to the more physical precipitation distribution scheme adopted in this work compared with the simpler scheme of B06, as described previously in section 3.

6. Errors as compared to observations

The impact of alternative schemes for cloud overlap modeling has been tested within the operational one-plus four-dimensional variational (1D+4DVAR) rain data assimilation at ECMWF (Bauer et al. 2006b,c). The test focuses on the calculation of first-guess radiance departures at SSM/I channel frequencies that are the differences between observed and modeled brightness temperatures. These have been produced from two different cloud overlap models: the current implementation of RTTOV, referred to as model 2C in this work, and the IC reference scheme. Contrary to the reference model of section 3, only 20 independent columns were taken to reduce computational cost. The error incurred by this smaller number of columns should be minimal (Fig. 3a).

The data were produced with the latest model version operated at ECMWF with a spatial resolution of 25 km that corresponds to a spectral wavenumber cutoff of 799. As part of the 1DVAR retrieval scheme, moist physics parameterizations produce vertical profiles of cloud liquid water and ice as well as liquid and frozen precipitation per model grid box. Given the definition of the SSM/I 3-dB footprint size and the spectral nature of the model, both model and observations can be assumed comparable in terms of their spatial representation of precipitation variability. The calculations have been performed from two days of assimilation for a total of four assimilation cycles with 12-h assimilation windows. Only data over ocean have been taken and

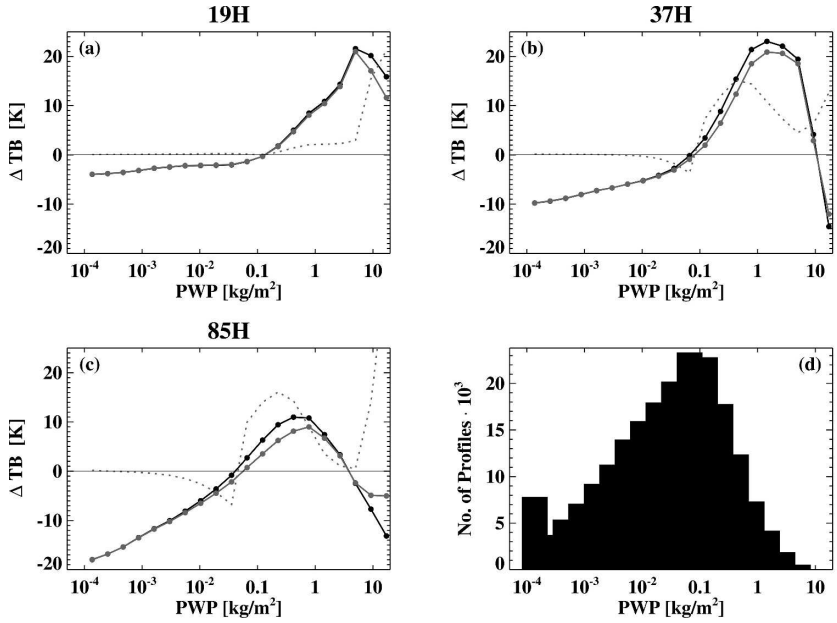

FIG. 8. Selected ECMWF model errors as compared with actual SSM/I observations vs PWP for a 2-day assimilation cycle using two different cloud overlap models: model 2C (black), native to RTTOV, and the reference IC approach with 20 columns (gray). Further details of the experiment are given in the text. Error statistics for channels (a) 19, (b) 37, and (c) 85 H. Solid lines denote the model biases, while the dotted line denotes the improvement of the bias for the IC model as compared to model 2C, multiplied by 5 for visibility (negative values imply a worsening of the bias). (d) The distribution of PWP for the roughly 200 000 profiles under consideration.

data screening, quality control, and thinning follow the operational procedure (Bauer et al. 2006a). The 1DVAR algorithm is activated only where the SSM/I observations are classified as cloudy/rainy. Roughly 200 000 profiles were processed from which the following evaluation is produced.

The salient results of this experiment are shown in Fig. 8, which shows the model minus observation brightness temperature (or bias) for three SSM/I channels: 19H, 37H, and 85H. These channels have the most sensitivity to clouds and precipitation in the atmosphere. The biases have been binned and plotted as a function of the column-integrated mass of precipitation, PWP. For reference, the bottom-right panel shows a histogram of PWP for these profiles. The main source of differences between observed and simulated radiances can be expected to be from the model representation of clouds and precipitation itself, that is, the presence or absence of clouds and the integrated cloud and precipitation water paths to which the SSM/I channels are most sensitive. The model tends to produce spurious cloud water and rain almost everywhere and thus overestimates rain coverage. On the contrary, because of the limited spatial resolution, rain intensity may be underestimated in severe storms (Chevallier and Bauer 2003).

The structure of the bias is similar for the different channels and for the two overlap models. At low values of PWP, the model is producing too little precipitation as compared with observations (which only include observations containing precipitation), leading to a negative model bias. The bias increases with PWP, as brightness temperatures generally increase with increasing PWP for the SSM/I frequencies, and the model is catching up to (and overtaking) the observations in terms of total precipitation. For the highest values of PWP, the model has generally produced much too much precipitation as compared with observations. However, the bias drops sharply at the highest values of PWP for all channels; this is because of the fact that the brightness temperatures themselves become very cold at the highest values of PWP, due to increased scattering from the frozen precipitation reflecting more cold space into the sensor. Thus, it is fair to say that the structure of the bias is exactly what one expects for a model that to some degree incorrectly predicts the amount of precipitation in any given profile.

The effects of the cloud overlap scheme are signifi-

cantly smaller as compared to the nonoverlap model errors (discussed above), but they are not completely negligible. Based on Fig. 8, we see that, for low values of PWP where the model produces too little precipitation, the overlap scheme actually makes things slightly worse. However, this does not necessarily indicate problems with the cloud overlap model; a more accurate overlap model does not always help a poor prediction. But for more moderate and higher values of PWP, greater than roughly 0.05–0.10 kg m^{-2}, the bias is always improved with the IC model regardless of the sign of the overall bias. These improvements (about 1–10 K) in average model error are roughly what is expected based on the theoretical results of section 5, and seem to imply that cloud overlap effects on the radiative transfer are indeed present in the observations.

Relative computational efficiency

When deciding whether or not to implement any new scheme within an operational context, computational speed is of great importance. In the following evaluation of the relative speeds of the various models described above, it should be noted that these results are for a single system only. Differences in the plane-parallel RT models, methods of calculating optical properties, and in other details of the actual RT code will in turn affect the results. Nevertheless, as the basic components of the calculations are always the same, such as partitioning of profiles into columns, evaluating optical properties, and performing the required plane-parallel RT calculations, these results are expected to be relatively typical.

The speeds of overlap models 2C, 3EQ, 2OP, and 3OP have been evaluated by inserting them into the RTTOV-8, version 7 publicly available radiative transfer code. As discussed previously, this code normally uses overlap model 2C, which requires one clear (nonscattering) and one cloudy (scattering) plane-parallel RT calculation. The clear RT calculation is performed on average 5 times faster than the cloudy RT calculation, where the latter includes the time necessary to calculate the optical properties of the scattering components such as cloud water, rain, and frozen precipitation. Relative to model 2C, model 3EQ takes roughly 2.35 times as long. This is because of the fact that it generally requires three scattering RT calculations, compared to only one for model 2C; it is not fully 3 times longer because of both the clear-sky RT calculation required for model 2C, as well as common overhead between the two approaches. Model 2OP is faster than model 3EQ, requiring only two scattering RT calculations, but it takes about 1.8 times as long as model 2C. Of this 75% slowdown, less than 10% is due to the partitioning of the scattering components within the two columns; the majority is due to the extra scattering RT calculation required. Model 3OP is similar in speed to model 3EQ (as they each require the same number of scattering RT calculations), taking about 2.5 times longer than model 2C.

7. Discussion

In this study we have presented a discussion of cloud overlap effects on microwave radiative transfer. To analyze these effects, a reference model was constructed that used many noninteracting subgrid-scale columns, independently evaluated using plane-parallel radiative transfer and averaged; clouds and precipitation were distributed using a physically based scheme. The errors of the reference model itself were evaluated through comparison to a more accurate 3D model and were found to be acceptable, though 3D errors become larger with increasing model resolution.

Next, cloud overlap errors were evaluated for several approximate yet fast models as compared to the reference model. It was found that the current operational scheme at ECMWF, dubbed model 2C in this work, can incur large errors due to cloud overlap, up to several tens of kelvin in some instances. An alternative two and three independent column scheme, referred to as the optimal approach, was presented that largely eliminates these errors with negligible increase in computational demand. The two-column optimal scheme, in particular, is roughly an order of magnitude more accurate than the current operational scheme, at the cost of being roughly 75% slower because it requires an extra scattering, plane-parallel RT calculation. Model 3OP is even more accurate, but is probably too computationally expensive for most applications.

Finally, the impact of alternative schemes for cloud overlap modeling was tested within the operational 1D + 4DVAR rain assimilation at ECMWF. Though the errors are mostly dominated by simple under- or overpredictions of precipitation combined with the one-sided precipitation filter (where the observations were screened for precipitation but the model was not), the effects of cloud overlap are discernible for profiles where both the model and observations show nonnegligible precipitation. Moreover, the magnitude of these effects is roughly consistent with the theoretical predictions of section 5, typically being several kelvin or more at 37 and 85 GHz.

Though certainly not the dominant source of error in simulated brightness temperatures, the cloud overlap effect can be substantial and should be addressed where possible. Operational centers attempting to assimilate

clouds and precipitation in radiance space may be affected by this error source, and some types of retrievals may be affected as well. Additionally, though not studied here, cloud overlap errors can of course be expected to occur in the infrared as well. A similar approach to the fast cloud overlap model presented here may be of potential benefit in the infrared as well, and warrants further study.

Acknowledgments. This work was partially supported by the Joint Center for Satellite Data Assimilation through NOAA cooperative agreement NA07EC0676.

REFERENCES

Bauer, P., P. Lopez, A. Benedetti, E. Moreau, D. Salmond, and M. Bonazzola, 2004: Assimilation of satellite-derived precipitation information at ECMWF in preparation of a future European contribution to GPM (EGPM). ESA Contract Final Rep. 17193/03/NL/GS, 85 pp.

——, ——, ——, D. Salmond, and E. Moreau, 2006a: Implementation of 1D+4D-Var assimilation of precipitation-affected microwave radiances at ECMWF. Part I: 1D-Var. *Quart. J. Roy. Meteor. Soc.,* **132,** 2277–2306.

——, ——, ——, ——, S. Saarinen, and M. Bonazzola, 2006b: Implementation of 1D+4D-Var assimilation of precipitation-affected microwave radiances at ECMWF. Part II: 4D-Var. *Quart. J. Roy. Meteor. Soc.,* **132,** 2307–2332.

——, E. Moreau, F. Chevallier, and U. O'Keefe, 2006c: Multiple-scattering microwave radiative transfer for data assimilation applications. *Quart. J. Roy. Meteor. Soc.,* **132,** 1259–1281.

Bennartz, R., and G. W. Petty, 2001: The sensitivity of microwave remote sensing observations of precipitation to ice particle size distributions. *J. Appl. Meteor.,* **40,** 345–364.

Chevallier, F., and P. Bauer, 2003: Model rain and clouds over oceans: Comparison with SSM/I observations. *Mon. Wea. Rev.,* **131,** 1240–1255.

Collins, W. D., 2001: Parameterization of generalized cloud overlap for radiative calculations in general circulation models. *J. Atmos. Sci.,* **58,** 3224–3242.

Deblonde, G., and S. J. English, 2001: Evaluation of the FASTEM-2 fast microwave oceanic surface emissivity model. *Tech. Proc. 11th Int. TOVS Study Conf.,* Budapest, Hungary, WMO and Cosponsors, 67–78.

——, J. F. Mahfouf, B. Bilodeau, and D. Anselmo, 2007: One-dimensional variational data assimilation of SSM/I observations in rainy atmospheres at MSC. *Mon. Wea. Rev.,* **135,** 152–172.

Di Michele, S., and P. Bauer, 2006: Passive microwave radiometer channel selection based on cloud and precipitation information content. *Quart. J. Roy. Meteor. Soc.,* **132,** 1299–1323.

English, S. J., R. J. Renshaw, P. C. Dibben, A. J. Smith, P. J. Rayer, F. W. Saunders, and J. Eyre, 2000: A comparison of the impact of TOVS and ATOVS satellite sounding data on the accuracy of numerical weather forecasts. *Quart. J. Roy. Meteor. Soc.,* **126,** 2911–2931.

Greenwald, T. J., R. Hertenstein, and T. Vukicevic, 2002: An all-weather observational operator for radiance data assimilation with mesoscale forecast models. *Mon. Wea. Rev.,* **130,** 1882–1897.

Heidinger, A. K., C. O'Dell, R. Bennartz, and T. Greenwald, 2006: The successive-order-of-interaction radiative transfer model. Part I: Model development. *J. Appl. Meteor. Climatol.,* **45,** 1388–1402.

Heilliette, S., and L. Garand, 2007: A practical approach for the assimilation of cloudy infrared radiances and its evaluation using AIRS similated observations. *Atmos.–Ocean,* in press.

Hogan, R. J., and A. J. Illingworth, 2000: Deriving cloud overlap statistics from radar. *Quart. J. Roy. Meteor. Soc.,* **126,** 2903–2909.

Hollinger, J. P., J. L. Pierce, and G. A. Poe, 1987: SSM/I instrument evaluation. *IEEE Trans. Geosci. Remote Sens.,* **28,** 781–790.

Jakob, C., and S. A. Klein, 2000: A parameterization of the effects of cloud and precipitation overlap for use in general-circulation models. *Quart. J. Roy. Meteor. Soc.,* **126,** 2525–2544.

Liebe, H. J., G. A. Hufford, and T. Manabe, 1991: A model for the complex permittivity of water at frequencies below 1 THz. *Int. J. Infrared Millimeter Waves,* **12,** 659–675.

Liou, K.-N., 2002: *An Introduction to Atmospheric Radiation*. Academic Press, 583 pp.

Mace, G. G., and S. Benson-Troth, 2002: Cloud-layer overlap characteristics derived from long-term cloud radar data. *J. Climate,* **15,** 2505–2515.

Morcrette, J. J., and C. Jakob, 2000: The response of the ECMWF model to changes in the cloud overlap assumption. *Mon. Wea. Rev.,* **128,** 1707–1732.

O'Dell, C. W., A. K. Heidinger, T. Greenwald, P. Bauer, and R. Bennartz, 2006: The successive-order-of-interaction radiative transfer model. Part II: Model performance and applications. *J. Appl. Meteor. Climatol.,* **45,** 1403–1413.

Oreopoulos, L., and M. Khairoutdinov, 2003: Overlap properties of clouds generated by a cloud-resolving model. *J. Geophys. Res.,* **108,** 4479, doi:10.1029/2002JD003329.

Petty, G. W., 1994: Physical retrievals of over-ocean rain rate from multichannel microwave imagery. Part I: Theoretical characteristics of normalized polarization and scattering indices. *Meteor. Atmos. Phys.,* **54,** 89–100.

Rosenkranz, P. W., 1998: Water vapor microwave continuum absorption: A comparison of measurements and models. *Radio Sci.,* **33,** 919–928.

Saunders, R., P. Brunel, S. J. English, P. Bauer, U. O'Keefe, P. Francis, and P. Rayer, 2005: RTTOV-8 science and validation report. NWP SAF Rep. NWPSAF-MO-TV-007, 46 pp.

Stephens, G. L., N. B. Wood, and P. M. Gabriel, 2004: An assessment of the parameterization of subgrid-scale cloud effects on radiative transfer. Part I: Vertical overlap. *J. Atmos. Sci.,* **61,** 715–732.

Tian, L., and J. A. Curry, 1989: Cloud overlap statistics. *J. Geophys. Res.,* **94,** 9925–9935.

Willen, U., S. Crewell, H. K. Baltink, and O. Sievers, 2005: Assessing model predicted vertical cloud structure and cloud overlap with radar and lidar ceilometer observations for the Baltex Bridge Campaign of CLIWA-NET. *Atmos. Res.,* **75** (3), 227–255.

Wu, X., and X.-Z. Liang, 2005: Radiative effects of cloud horizontal inhomogeneity and vertical overlap identified from a monthlong cloud-resolving model simulation. *J. Atmos. Sci.,* **62,** 4105–4112.